CHEMISTRY OF MATERIALS

ARTICLE

pubs.acs.org/cm

Newkome-Type Dendron-Stabilized Gold Nanoparticles: Synthesis, Reactivity, and Stability

Tae Joon Cho,[†] Rebecca A. Zangmeister,[†] Robert I. MacCuspie,[†] Anil K. Patri,[‡] and Vincent A. Hackley*[,†]

[†]Material Measurement Laboratory, National Institute of Standards and Technology, Gaithersburg, Maryland 20899, United States

[‡]Nanotechnology Characterization Laboratory, Advanced Technology Program, SAIC-Frederick, Inc., National Cancer Institute at Frederick, Frederick, Maryland 21702, United States

Supporting Information

ABSTRACT: We report the synthesis and evaluation of four Newkome-type dendrons, G1-COOH, G2-COOH, SH-G1-COOH, and TA-G1-COOH, and their respective gold–dendron conjugates, where GX represents the generation number. G1- and G2-COOH are two-directional symmetric dendrons that have cystamine cores containing a disulfide group. SH-G1-COOH was prepared by treatment of G1-COOH with dithioerythritol to yield a free thiol group to replace the disulfide linkage. TA-G1-COOH has a thioctic acid moiety, which is a five-membered ring containing a disulfide group that cleaves to produce two anchoring thiols to bond with the gold surface. All dendrons have peripheral carboxylate groups to afford hydrophilicity and functionality. Gold nanoparticle conjugates were prepared by reaction of each dendron solution with a suspension of gold colloid (nominally 10 nm diameter) and purified by stirred cell ultrafiltration. Chemical structures were confirmed by ^{1}H and ^{13}C nuclear magnetic resonance spectroscopy and matrix assisted laser desorption/ionization time-of-flight mass spectrometry. Particle size and surface plasmon resonance of the conjugates were characterized by dynamic light scattering (DLS) and UV–vis spectroscopy, respectively. X-ray photoelectron spectroscopy (XPS) was utilized to confirm covalent bonding between the thiols on the dendron and the gold surface. XPS also revealed changes in the S/Au intensity ratio as a function of the dendron chemical structure, suggesting steric effects play a role in the reaction and/or conformation of dendrons on the gold surface. The colloidal and chemical stability of the conjugates as a function of temperature, pH, and suspending medium, and with respect to chemical resistance toward KCN, was investigated using DLS and UV–vis absorption.

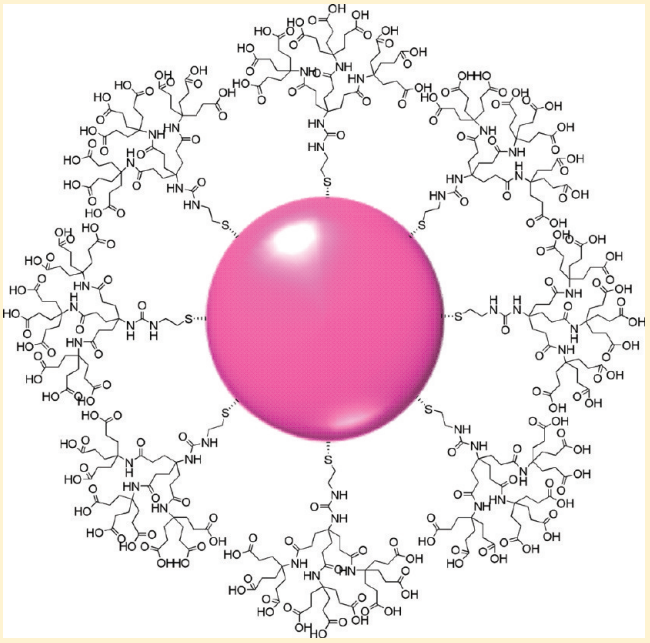

KEYWORDS: gold nanoparticle, dendrimer, dendron, conjugate, characterization, stability

INTRODUCTION

During the past decade, the development and study of nanoparticles (NPs) and their functionalized conjugates have enjoyed a rapidly growing dominance in the field of nanotechnology.[1−4] In particular, gold nanoparticles (AuNPs) have demonstrated immense potential for applications including drug delivery,[5−9] diagnostics and imaging,[10−14] sensors,[1,14−20] and therapeutics.[8,9,13,21−23] The appeal of AuNPs derives primarily from their chemical stability, biocompatibility, commercial availability, and the ease with which they can be conjugated with a broad range of functional molecules. The ability to synthesize AuNPs in a wide range of sizes and morphologies is also beneficial.[24−31] Numerous publications have documented the flexibility of AuNPs with respect to ligand conjugation[1,9,24,32] and applications based on their physicochemical properties.[9,24,33−40]

Dendrimers are monodisperse, hyperbranched nanoscale molecular architectures possessing a unique and well-defined structure containing connectors and building blocks arranged around a small molecule or a linear polymer core.[41,42] Considered as a subclass of dendrimers, dendrons are differentiated as wedge-shaped individual branching structures coupled to a single reactive functional unit, whereas the term dendrimer is frequently used to indicate spherically symmetric structures. The wedge-like dendron structure allows one to graft the molecule directly to a

Received: February 25, 2011
Revised: April 12, 2011
Published: April 26, 2011

surface. Since the successful development of dendrimer-encapsulated NPs by Tomalia[43] and Crooks,[44,45] dendrimers, as a class of nanomaterials, have been widely utilized in nanotechnology.[46] The subsequent development of dendrimer-based nanocomposites[47−61] and nanoconjugates[62−78] is attractive because of their unique structures and properties, as well as their highly controllable internal and/or external functionalities and dimensions.

Here we report the development and properties of AuNP-dendron conjugates (hereafter referred to simply as conjugates). The conjugates were conceived as prototypes for investigations of NP-biological interactions and as candidate nanoscale reference materials. In particular, dendron encapulated AuNPs permit variation of surface-active groups while maintaining a common underlying core/shell platform. This research approach allows for: (1) better control over size and size distribution of conjugates due to complete separation of the AuNP synthesis and surface encapsulation processes; citrate-capped AuNPs with tightly controlled and well-characterized core sizes are used in the present study, (2) improved stability of AuNPs in biologically relevant media, including physiological saline levels, by grafting water-soluble dendrons onto the AuNP surface, and (3) provision of potentially useful and unique templates for biological applications because of the surface site density and range of possible functional groups afforded by the dendron conjugates.

In the present study we focus on Newkome-type dendrons[41] that possess a 1 (amine) → 3 (esters) branched structure, and which are used in the divergent synthesis of a family of amide connected dendrimers. The facile conversion of amine to the corresponding isocyanate has expanded its utilitarian appeal. The peripheral esters are easily hydrolyzed to carboxylic acids; this consequently allows for enhanced solubility in aqueous media as well as increased reactivity with other dendrons to afford either additional dendron generations or functionality for use in medical applications, such as coupling with biologically active species. Here we have prepared Newkome-type dendrons designed with consideration of the sulfide content (ligand exchange onto the gold core), the generation number (determines the shell thickness in the core/shell conjugate structure), steric effects that would inhibit reaction and impact conformation, hydrophilicity of the dendron, and surface functionality of the termini. Citrate-capped AuNPs nominally 10 nm in size were selected for the gold core in the preparation of the conjugates. Physicochemical properties of the resulting conjugates were characterized by dynamic light scattering (DLS), UV−vis spectroscopy, atomic force microscopy (AFM), and X-ray photoelectron spectroscopy (XPS). Additionally, the colloidal and chemical stability of the conjugates as a function of temperature, pH, and suspending medium (including physiological saline levels), and with respect to chemical resistance against KCN-induced Au dissolution, was investigated using DLS and UV−vis absorption.

EXPERIMENTAL METHODS

Reagents and Instrumentation. Cystamine dihydrochloride (98%), dithioerythritol (DTE, 99%), thioctic acid (99%), formic acid (≥96%), *N*,*N*′-dicyclohexylcarbodiimide (DCC, 99%), 1-hydroxy-1H-benzotriazole hydrate (1-HOBT), citric acid (99.5%), sodium citrate dehydrate (≥99%), sodium sulfate anhydrous (Na_2SO_4, ≥ 99%), sodium chloride (NaCl, 99.5%), potassium cyanide (KCN, ≥ 96%), triethyamine (Et_3N), and ACS-grade solvents including tetrahydrofuran (THF), dimethylformamide (DMF), dichloromethane (CH_2Cl_2), hexanes, ethyl acetate, and methanol (MeOH) were obtained from Sigma-Aldrich (St. Louis, MO). (Certain trade names and company products are mentioned in the text or identified in illustrations in order to specify adequately the experimental procedure and equipment used. In no case does such identification imply recommendation or endorsement by National Institute of Standards and Technology or the Department of Health and Human Services, nor does it imply that the products are necessarily the best available for the purpose.) Ditert-butyl-4-[2-(tert-butoxycarbonyl)ethyl]-4-isocyanato-1,7-heptanedicarboxylate (Weisocyanate) and Ditert-butyl-4-[2-(tert-butoxycarbonyl)ethyl]-4-amino-1,7-heptanedicarboxylate (Behera's amine) were obtained from Frontier Scientific, Inc. (Logan, Utah). Phosphate buffered saline (PBS10X) was obtained from HyClone (Logan, Utah). All chemicals were used without further purification. Column chromatography was conducted using silica gel (Sigma-Aldrich, 70−230 mesh, 60 Å) or alumina (basic, Brockmann I, ∼150 mesh, 58 Å) with the appropriate solvent mixture. Citrate stabilized gold colloid (10 nm, nominal particle diameter) was obtained from Ted Pella, Inc. (Redding, CA; manufactured by BBI-International, UK). Deionized water (18.2 MΩ·cm) was produced by an Aqua Solutions (Jasper, GA) Type I DI (RO+DI) reagent grade water purification system.

^1H and ^{13}C nuclear magnetic resonance (NMR) spectra were obtained on a JEOL GSX270 FT-NMR (JEOL USA Inc., Peabody, MA) and were recorded at 270 and 67.5 MHz, respectively. A Voyager-DE Pro matrix assisted laser desorption/ionization time-of-flight (MALDI-TOF) mass spectrometer (Applied Biosystems, Foster City, CA) was utilized for determination of molecular mass. The accelerating voltage was 20 kV, guide wire 0.002% and grid voltage 75%. The instrument was operated in reflectron mode under positive ion conditions. A nitrogen laser was used at 337 nm with 150 laser shots averaged per spectrum. The matrix used for all experiments was 2,5-dihydroyxbenzoic acid (Sigma-Aldrich). pH was recorded with an Orion 520A using an Thermo Orion model 9157BN pH triode. UV−vis spectra were collected on a Perkin-Elmer (Waltham, MA) Lambda 750 spectrophotometer. DLS was collected on a Malvern Instruments (Westborough, MA) Zetasizer Nano operated in 173° backscatter mode with a laser wavelength of 633 nm. AFM images were obtained in tapping mode using a Veeco Instruments (Santa Barbara, CA) Dimension 3100 instrument with a Nanoscope V controller. XPS spectra were obtained with an AXIS UltraDLD (Kratos Analytical, Manchester UK) and used for the analysis of S/Au ratio and to confirm bonding with the Au surface.

Characterization and Stability Study. DLS procedures followed the National Institute of Standards and Technology (NIST) − Nanotechnology Characterization Laboratory (NCL) protocol[79] (freely available online) with z-average values reported as the mean of no less than five measurements plus or minus one standard deviation. UV−vis spectra were collected in UV-transparent disposable plastic semimicrocuvettes (Brandtech, Inc., Essex, CT) with a 1 cm path length, and requiring 1 mL to fill the light path of the UV−vis spectrometer used. The spectrometer was a split-beam style equipped with an 8 + 8 cell changer and water-jacketed temperature control. AFM images were obtained by intermittent contact or tapping mode. Cantilevers with nominal spring constants of 7.4 N/m, and a tip radius of curvature of approximately 8 nm were used to collect all images. Nanoparticle samples were deposited onto aminated surfaces (Si chips treated with 3-aminopropyldimethoxyethoxysilane) to prevent drop-pinning or drying-induced aggregation. XPS measurements were made with an AXIS UltraDLD (Kratos Analytical, Manchester, U.K.) system using monochromatic Al Kα radiation at an X-ray power of 150 W. AuNP-dendron conjugates were concentrated by centrifugation and drop cast onto commercially available indium foil for analysis. All XPS measurements were performed on freshly prepared samples and each sample was measured at three positions within a single sample spot. The uncertainty of XPS measurements was recorded as standard deviation well as DLS study. Shelf life and stability under various temperatures of AuNP-dendron

Scheme 1. Synthesis of Two-Directional Cystamine Core Dendrons 4 (G1-COOH) and 7 (G2-COOH)[a]

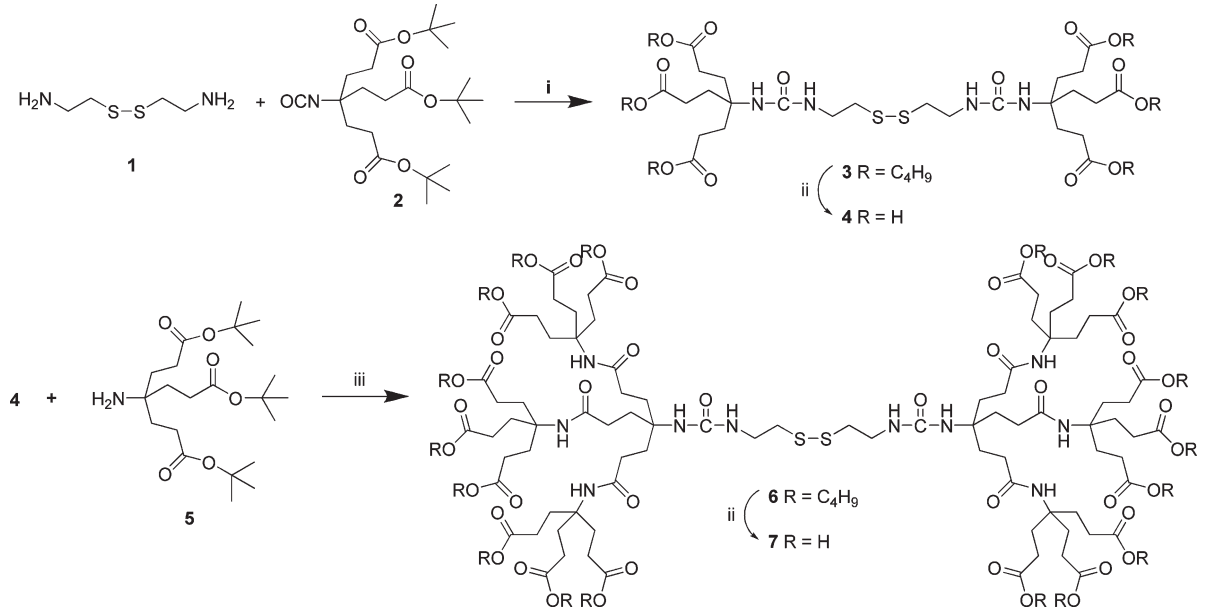

[a] Reagents and conditions: (i) Et_3N, THF, r.t., 12 h; (ii) formic acid, r.t., overnight; (iii) DCC, 1-HOBT, DMF, r.t., overnight.

Scheme 2. Preparation of One-Directional Dendrons 8 (SH-G1-COOH) and 11 (TA-G1-COOH)[a]

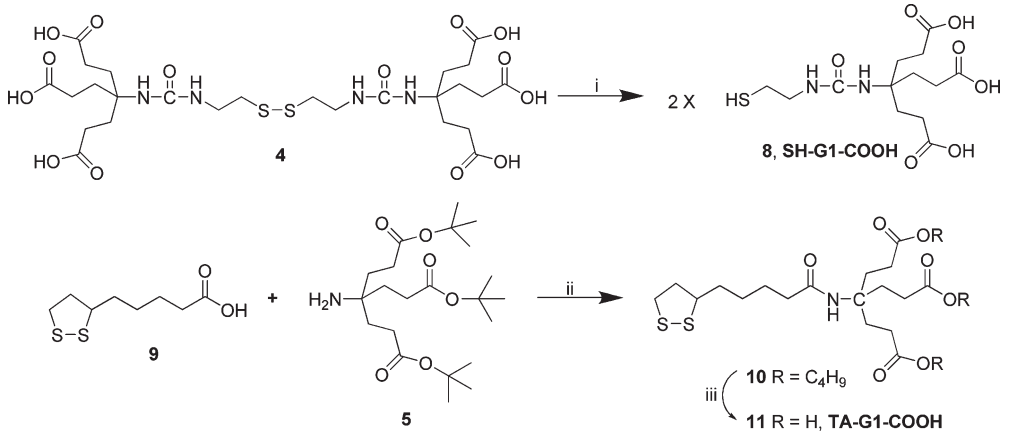

[a] Reagents and conditions: (i) DTE, citrate buffer (pH 6.2), 55 °C, overnight; (ii) DCC, 1-HOBT, THF, r.t., overnight; (iii) formic acid, r.t., overnight.

conjugates were investigated as they were without dilution by DLS, and UV−vis measurements. On the other hand, the stability studies in media such as PBS, various pHs, and 2.0 mmol/L KCN solutions were conducted with dilution factor (f) 10 by DLS and UV−vis as well. The pH values were adjusted by mixing of 50 mmol/L HCl and NaOH solution. All DLS and UV−vis measurements were conducted at 20 ± 0.1 °C unless noted.

RESULTS AND DISCUSSION

Preparation of Dendrons and AuNP−Dendron Conjugates. As summarized in Schemes 1 and 2 and Figure 1, we have synthesized four Newkome class dendrons, G1-COOH 4, G2-COOH 7, SH-G1-COOH 8, and TA-G1-COOH 11 (Schemes 1 and 2) as targeted dendrons for the preparation of conjugated AuNPs.

G1- and G2-COOH (Scheme 1) are 2-directional dendrons that have cystamine cores containing a disulfide group. Cystamine 1 was treated with 2 equivalents of Weisocyanate[80] 2 in the presence of triethylamine (Et_3N) in tetrahydrofuran (THF) to afford a urea adduct (90% yield) 3. Hydrolysis of G1-hexa-*tert*-butylester 3 with formic acid at ambient temperature overnight produced the hexacarboxylic acid dendron, G1-COOH 4 with 95% yield. For the preparation of G2-COOH 7, hexaacid 4 was treated with 6 equiv. of Behera's amine[81] 5 in the presence of *N*, *N*′-dicyclohexylcarbodiimide (DCC) and 1-hydroxy-1*H*-benzotriazole (1-HOBT) in dimethylformamide (DMF) to yield (37%) G2 predendron 6, which was then deprotected with formic acid overnight at room temperature to give G2-COOH 7 quantitatively.

To reduce steric effects on the conjugation reaction, we prepared one-directional monothiol dendron SH-G1-COOH 8

dx.doi.org/10.1021/cm200591h |*Chem. Mater.* 2011, 23, 2665–2676

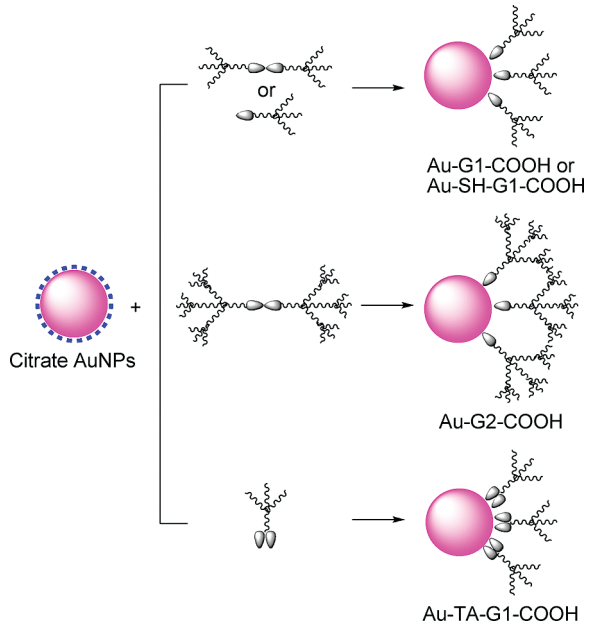

Figure 1. Cartoon depictions of conjugates and their preparation processes based on reacting dendron solutions with citrate-stabilized AuNP suspensions at room temperature for 5 h; the relative sizes are not to scale and the number of molecules shown is not a realistic reflection of the actual surface site density.

(Scheme 2) by reduction of the disulfide group on G1-COOH 4 with 1.1 equivalents of dithioerythritol (DTE). As described above, we factored in the number of sulfides on a single molecular unit, as well as steric effects, in dendron design. This led us to synthesize TAG1-COOH 11 (Scheme 2) as a "di-anchored" dendron for conjugate formation. Thioctic acid (TA) 9, the starting material, which is a 5-membered ring containing a disulfide group, provides the two anchoring thiols to react with the gold surface, and was coupled with Behera's amine 5 under similar amidation conditions to produce thioctic-tri*tert*-butyl ester 10 (81% yield). The deprotection reaction of 10 was conducted under similar hydrolysis conditions to afford the targeted dianchor dendron TA-G1-COOH 11 with 42% yield.

The conjugates Au-G1-COOH, -G2-COOH, -SH-G1-COOH, and -TA-G1-COOH (Figure 1) were prepared by mixing each dendron solution into a suspension of citrate stabilized gold colloids (nominally 10 nm diameter), followed by purification using stirred cell ultrafiltration.

Characterization of Conjugates. DLS, UV−vis, XPS, and AFM were employed to determine the physicochemical properties of conjugates; the results are summarized in Table 1.

UV−vis absorbance spectra showed that all conjugates exhibit an absorption peak near $\lambda_{max} \approx 520$ nm, which is characteristic of the surface plasmon resonance (SPR) band for AuNPs in this size range.[37] Compared to the SPR of citrate-capped AuNPs ($\lambda_{max} \approx 518$ nm), the conjugates exhibited a slight red shift ($\Delta\lambda = 2-4$ nm) due to surface modification by ligand exchange. Additionally, the absence of a large red shift of the SPR absorbance band demonstrates that there is no significant particle aggregation occurring during the conjugate formation process.[82]

From DLS one obtains the equivalent hydrodynamic diameter (d_h) associated with the conjugates. Briefly, DLS measures the diffusion coefficient (D_z) of particles undergoing random thermal motion, and by application of the Stokes−Einstein relationship (eq 1) d_h is obtained.[83]

Table 1. Summary of Physicochemical Characterization Results for AuNP−Dendron Conjugates Obtained by DLS, UV−Vis Spectroscopy, and XPS[a]

AuNP species	Z-average size (d_z, nm)	SPR (λ_{max}, nm)	relative surface coverage
Citrate AuNP	12.2 ± 0.1	518	0
Au-G1-COOH	15.2 ± 0.1	520	0.38 ± 0.23
Au-G2-COOH	17.4 ± 0.1	521	0.19 ± 0.09
Au-SH-G1-COOH	15.1 ± 0.1	520	0.76 ± 0.04
Au-TA-G1-COOH	15.2 ± 0.1	522	0.93 ± 0.03
Au-MUA	22.3 ± 0.2	523	1.0 ± 0.07

[a] Relative surface coverage was calculated based on S/Au intensity ratios for each conjugate as determined by XPS, and setting the S/Au intensity ratio measured for mercaptoundecanoic acid (MUA) conjugated AuNPs to 1.0 as a benchmark value. DLS uncertainty intervals represent 1 standard deviation based on replicate measurements conducted under repeatability conditions.

$$d_h = \frac{kT}{3\pi\mu D_z} \quad (1)$$

Here, k is Boltzmann's constant, μ is viscosity of the medium, and T is the absolute temperature of measurements. The z-average size is obtained by application of the cumulants method,[84] which assumes a single size Gaussian mode. It is also possible to derive a size distribution by application of a suitable inversion algorithm with appropriate smoothing in combination with non-negative least-squares (NNLS) fitting to the measured correlation function.

All dendron conjugates showed appropriate z-average sizes (Table 1), which were slightly larger than the native citrate-capped AuNPs. The derived DLS size distributions were found to be monomodal with a relatively narrow distribution, as shown in Figure 2.

The measured z-average size of all generation 1 dendron conjugates (**Au-G1-COOH**, **-SH-G1-COOH**, and **-TA-G1-COOH**) was about 15 nm, which is approximately 3 nm larger than the native citrate-capped AuNPs. The **Au-G2-COOH** showed an increase in size of ~5 nm relative to the native material. These results are evidence of successful dendron coupling onto the AuNPs, and the consistently narrow monomodal distributions confirm the absence of aggregation. Moreover, the polydispersity index derived from the second-order coefficient of the cumulants analysis obtained by DLS did not increase significantly following the formation of AuNP conjugates; this result further supports the conclusion that conjugation is homogeneous and largely free from agglomeration effects.[85] Furthermore, AFM images and histograms of size distributions (see the Supporting Information, Figure S1) confirm the lack of agglomerates or aggregates following the ligand exchange reaction and subsequent purification step in all samples, and the uniformity of conjugate size in most samples. Notably, the z-average size for the **Au-MUA** conjugate (where MUA is 11-mercaptoundecanoic acid) is larger ($d_z = 22.3$ nm) compared with the dendron conjugates. This can likely be traced to the different preparation conditions required for conjugation with the sparingly water-soluble MUA and/or purification process using diafiltration (see the Supporting Information), and probably indicates some degree of agglomeration is present in this material; however, since the **Au-MUA** is

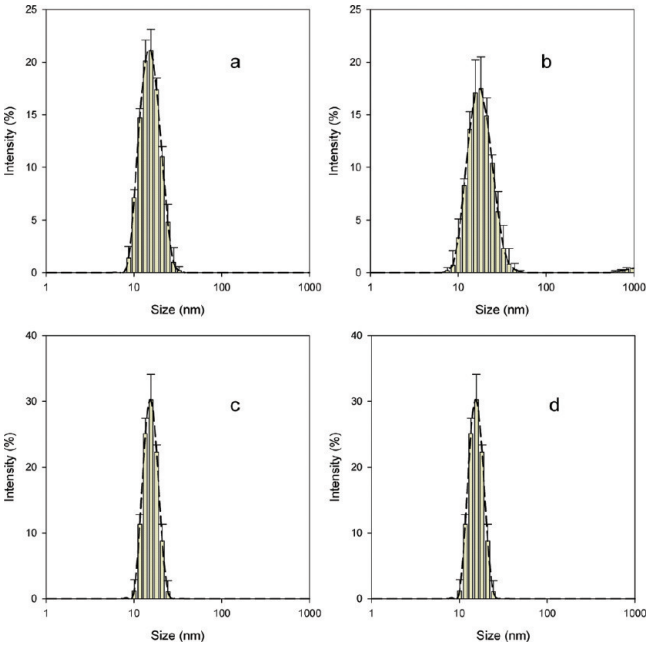

Figure 2. DLS intensity-weighted size distributions obtained for Au conjugates using NNLS: (a) **Au-G1-COOH**, (b) **Au-G2-COOH**, (c) **Au-SH-G1-COOH**, and (d) **Au-TA-G1-COOH**.

used solely for the purpose of benchmarking the XPS results for S/Au ratio comparisons, the size difference is inconsequential.

XPS has been used previously to study the chemical bonding between planar gold and gold nanoparticle surfaces with thiol modifiers.[86−88] Here we use XPS for the characterization of dried films of AuNP conjugates that were drop-cast onto indium foil in order to confirm the presence of the chemical functional groups expected from the ligand exchange reaction and also to probe the S−Au bonding interaction. XPS spectra were collected for dried films of citrate-stabilized AuNPs and **Au-G1-COOH**, **Au-G2-COOH**, **Au-SH-G1-COOH**, **Au-TA-G1-COOH**, and **Au-MUA** conjugate materials. Spectra obtained on citrate-stabilized and MUA modified AuNPs were as expected and similar to those reported previously in the literature.[86,88]

High-resolution spectra were collected for the C 1s, N 1s, Au 4f and S 2p energy regions. The presence and shape of peaks collected in these regions confirm the presence of the AuNP modifiers and also, in the case of the S 2p region, indicate how the S is bound to the AuNP and to what degree. Regions scanned in these areas did not vary appreciably between the samples analyzed; representative region scans taken on the **Au-G1-COOH** conjugates are shown in Figure 3.

The C 1s peak envelope can be fit with three peaks associated with elemental carbon (C−C species at 284.9 eV), carbon bound to a single oxygen or single nitrogen atom (C−O or C−N species at 286.0 eV), and carbon bound to two oxygen atoms (C═OOH species at 288.9 eV).[89] The presence of these peaks corresponds well with those species expected to be observed from the chemical structure of the dendron modifiers. The N 1s region exhibits one peak at 399.5 eV, associated with amide groups. The Au 4f region exhibits a pair of peaks at 83.9 and 87.6 eV assigned to the Au $4f_{7/2}$ and Au $4f_{5/2}$ peaks, respectively, originating from the AuNP cores.[89] The S 2p region peak envelope can be fit with two sets of peaks. Peaks associated with the S $2p_{3/2}$ and S $2p_{1/2}$ photoelectron pair originating from S

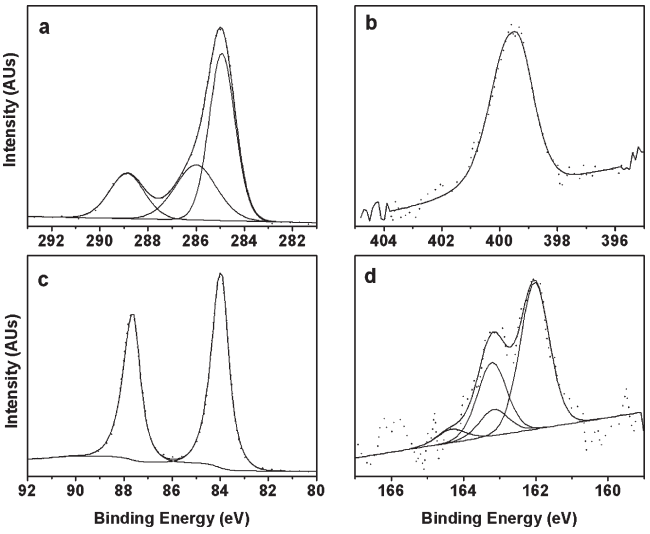

Figure 3. Representative high-resolution XPS spectra for (a) C 1s, (b) N 1s, (c) Au 4f, and (d) S 2p regions collected for **Au-G1-COOH** conjugates. The peak shape was consistent across samples.

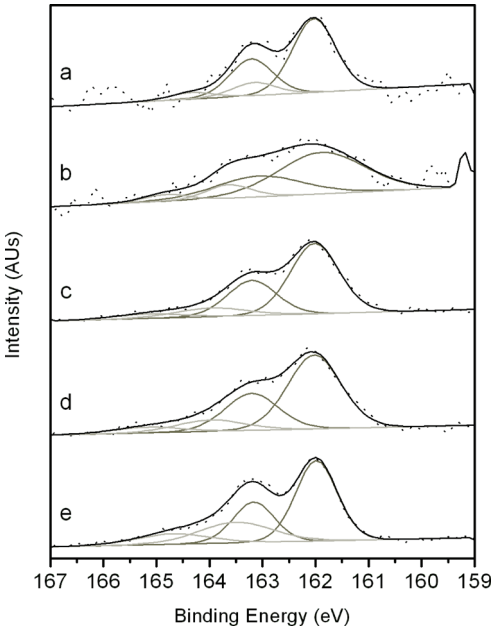

Figure 4. High-resolution XPS spectra for the S 2p region collected for (a) **Au-G1-COOH**, (b) **Au-G2-COOH**, (c) **Au-SH-G1-COOH**, (d) **Au-TA-G1-COOH**, and (e) **Au-MUA**.

atoms bound to Au are observed at 162.0 and 163.2 eV, respectively, and make up the majority of the S 2p signal. Peaks associated with the S $2p_{3/2}$ and S $2p_{1/2}$ photoelectrons of S atoms not bound to Au are observed at 163.9 and 165.2 eV, respectively, and are minor components.[90] Detection of photoelectrons originating from unbound S groups in thiolate films is not uncommon for thiol modifiers that contain carboxylic acid end groups due to hydrogen bonding between the terminal groups of the bound layer and carboxylic acid groups on free modifier molecules in the bulk.[86,88] Contribution of the signal originating from the unbound S species is eliminated from the calculation of S to Au intensity ratios used to determine relative

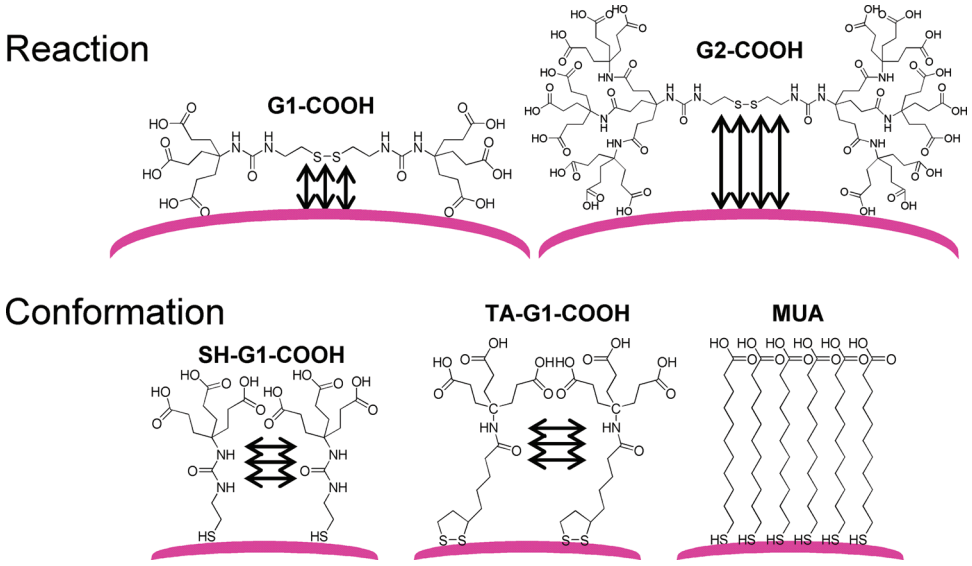

Figure 5. Cartoon depiction showing hypothesized steric effects for dendrons during conjugate formation.

surface coverage values by only considering signal contribution from bound S species, as will be discussed below.

The S regions were compared for all materials analyzed and are shown in Figure 4. The shape of the S 2p peak envelopes are nearly identical for all species.

The position of the S $2p_{3/2}$ peak is the same (162.0 eV) in all cases; and the peak intensities originating from S atoms bound to Au atoms as compared with S atoms not bound to Au atoms is similar in all cases. The intensity of the S 2p peaks measured on the different conjugates cannot be directly compared because the signal intensities obtained were influenced by the density of the sample deposits prepared for analysis; one can observe poorer signal-to-noise ratios for S peaks obtained for the **Au-G1-COOH** and **Au-G2-COOH** samples, which is attributed to a lower surface density as a result of the following analysis. What can be reliably compared is the intensity ratio of the S $2p_{3/2}$ peak intensity of the bound sulfur species to the Au $4f_{7/2}$ peak intensity measured on a single sample. This S/Au ratio is not affected by slight differences in the sample deposit density. The use of the S/Au ratio as a metric for molecular surface coverage on nanoparticles was first reported by Weisbecker et al.[90]

Au-MUA conjugates were prepared as a benchmark material to represent maximal molecular surface coverage for comparison with the dendron conjugates. Although absolute coverage was not determined, our approach enables a comparison of relative coverage for the various AuNP modifications explored here. The relative coverage was calculated by first determining the S/Au ratio for each sample by dividing the intensity of the S $2p_{3/2}$ peak for the bound species (162.0 eV) by the intensity of the Au $4f_{7/2}$ peak, and then dividing that ratio by the ratio obtained for the **Au-MUA** sample. The resulting values are listed in Table 1 and reveal that steric effects influence the molecular packing of the dendron modifiers on the AuNP surface. As shown in scheme 1, G1-COOH **4** and G2-COOH **7** are two-directional dendrons. In G1-COOH and G2-COOH dendrons, the cystamine active site core is located in the middle of the chains, and is thus hindered from contacting the Au surface by the side branches. Hypothesized steric interactions are depicted in Figure 5 for different dendron conjugates.

This steric effect resulted in low relative surface coverage values for **Au-G1-COOH** (0.38), and **Au-G2-COOH** (0.19) samples. Alternatively, SH-G1-COOH **8** and TA-G1-COOH **11** are 1-directional dendrons (Scheme 2) and the active site in SH-G1-COOH (thiol), or TA-G1-COOH (disulfide) is fully accessible for contact with the Au surface; this resulted in higher calculated surface coverage for conjugates of **Au-SH-G1-COOH** (0.76) and **Au-TA-G1-COOH** (0.93). Interestingly, even though the SH-G1-COOH dendron is free from steric hindrance, its AuNP conjugate has a lower S/Au ratio than **Au-MUA**. This can be explained by the fact that MUA molecules are able to pack more tightly than the 1 → 3 branched dendron molecules during conjugation. The relative surface coverage for the **Au-TA-G1-COOH** approached the maximum value; it is believed that the disulfide linkage is severed forming two anchoring S−Au bonds leading to high occupancy based on the S/Au ratio despite conformational steric hindrance between intermolecular branches. These overall characterization results supported successful thiolated dendron conjugation including characteristic SPR absorbance, appropriate sizes, narrow and monodisperse size distributions as well as the initial hypothesis that the steric effects induced from dendron structure would influence the AuNP-dendron conjugate formation itself.

Stability Studies. The stability of the AuNP conjugates under various conditions is an important issue for potential biological applications as well as for long-term storage and their possible use as candidate nanoscale reference materials.

Temperature-dependent stability studies were conducted from (20 to 60) °C using DLS and UV−vis spectroscopy. Samples were incubated for 30 min at each temperature before measurements were initiated. As shown in Figure S2 (see the Supporting Information), the *z*-average size measured by DLS (see Figure S2a in the Supporting Information) and SPR bands obtained from UV−vis absorption (see Figure S2b in the Supporting Information) for all conjugates are constant over the range of temperatures probed. This demonstrates that the conjugates are highly stable at temperatures relevant to biological applications. The observed temperature stability is not surprising since the commercial citrate-capped AuNPs exhibit similar stability in this range, so results demonstrate that conjugate formation does not reduce thermal stability of the native material.

To evaluate their stability in different media, we diluted conjugates (dilution factor f = 10) into deionized (DI) water (as a

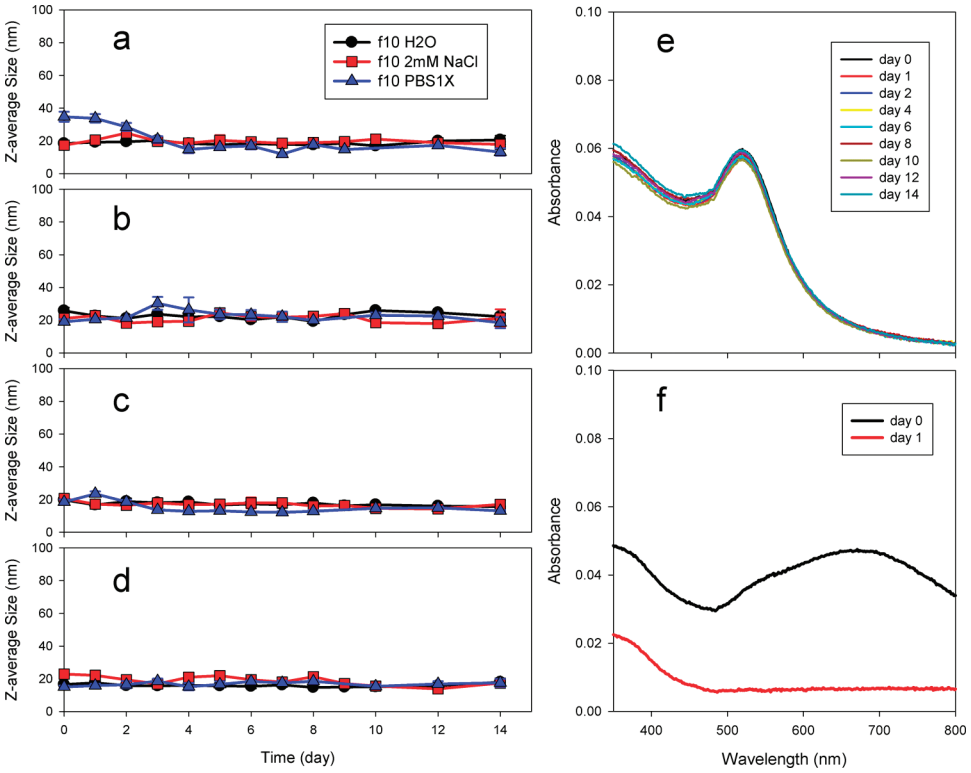

Figure 6. (Left): Stability of conjugates in different media (dilution factor $f = 10$): in DI water (circles), in 2 mmol/L NaCl (squares), and in PBS (triangles) monitored by DLS over 2 weeks. Results shown for (a) **Au-G1-COOH**, (b) **Au-G2-COOH**, (c) **Au-SH-G1-COOH**, and (d) **Au-TA-G1-COOH**. (Right): Stability of **Au-SH-G1-COOH** in (e) PBS by UV−vis over 2 weeks, (f) citrate AuNP over 1 day in PBS at 20 °C.

control), 2.0 mmol/L NaCl, and phosphate buffered saline (PBS), then monitored using DLS and UV−vis absorbance. The hydrodynamic size of the conjugates in DI water and 2.0 mmol/L NaCl remained unchanged for at least 2 weeks (Figure 6).

Similar behavior was exhibited in PBS, which contains a physiological (isotonic) saline concentration (154 mmol/L NaCl). By contrast, the native citrate-capped AuNPs aggregate immediately and "crash out" forming black precipitates when diluted into PBS. Monitoring of the SPR band further confirmed the stability of the dendron conjugates in the three tested media (Figure 6e, represented by **Au-SH-G1-COOH** in PBS) and demonstrated the lack of stability for the native citrate-capped AuNPs (Figure 6f). These results are encouraging because stability in physiologically relevant media, where saline levels are high, is a significant issue for the use of AuNPs in biological applications and assays. We therefore view stability in PBS as an initial screening test for compatibility with physiological conditions.

The substantial improvement in stability in high saline media for conjugates, relative to citrate-capped AuNPs, can be attributed to the inherent solubility associated with the dendron molecular structure[91] coupled with the addition of a salt-insensitive steric repulsive force arising from the bulky, and strongly anchored, dendrons grafted to the Au surface. Among the conjugates, **Au-SH-G1-COOH** exhibited the most stable behavior in PBS (see Figure S3 in the Supporting Information), with the stability order (based on UV−vis spectral analysis) as follows: **Au-SH-G1-COOH** > **-TA-G1-COOH** ≥ **-G2-COOH** > **-G1-COOH**. This order suggests that increased density of S bonding on the Au surface could increase the stability in physiologically relevant media.

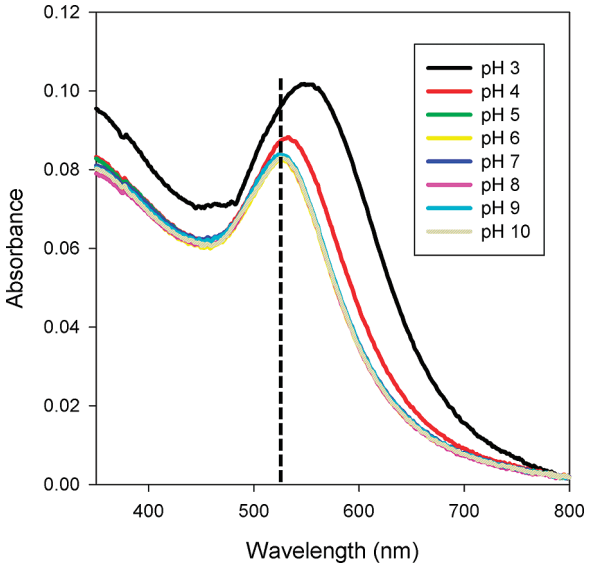

Figure 7. SPR bands for the **Au-TA-G1-COOH** conjugate as a function of pH ($f = 10$). The behavior exhibited here is generically similar for all dendron conjugated AuNPs.

The pH stability is an important consideration for therapeutic applications of orally administered NPs, as well as other potential biomedical uses.[92] For instance, highly acidic conditions exist in the human stomach (approaching pH 2), while proceeding into and through the intestines, the pH gradually increases to mildly basic conditions (≈ pH 8). Lysosomes within mammalian cells

dx.doi.org/10.1021/cm200591h |*Chem. Mater.* 2011, 23, 2665–2676

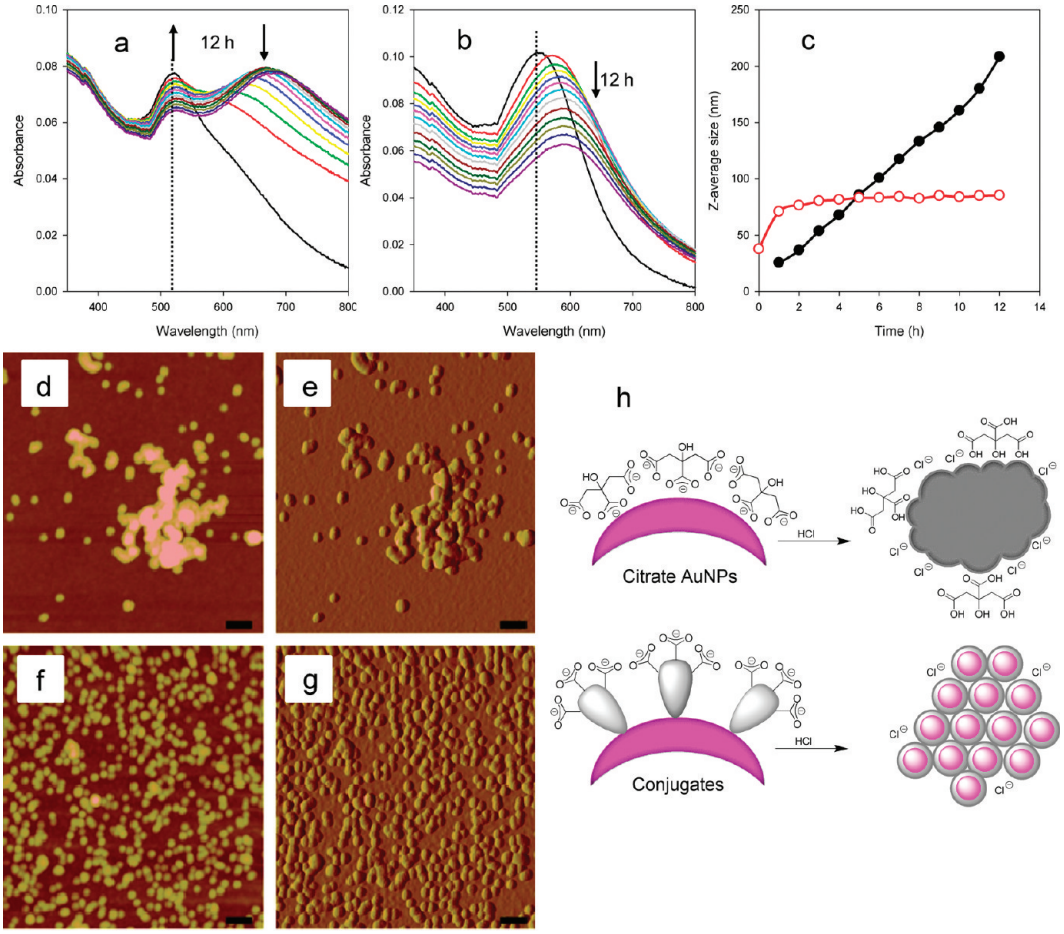

Figure 8. Time-dependent studies of AuNPs in acidic media (pH 3). UV−vis absorbance spectra for (a) citrate-capped AuNPs and (b) **Au-TA-G1-COOH**; vertical marker (•••) indicates 520 nm. (c) *Z*-average size versus time for (●) citrate-capped AuNPs and (○) **Au-TA-G1-COOH**. (d, f) AFM height and (e, g) amplitude images of citrate-capped AuNPs (d, e) and **Au-TA-G1-COOH** (f, g) after 48 h at pH 3; scale bars are 100 nm, *z*-scale is 20 nm for height images. (h) Cartoon depiction of cluster formation mechanism comparing citrate-capped AuNPs and AuNP−dendron conjugates under acidic conditions.

are characterized by moderately acidic pH levels between 4 and 5, and the pH of the bloodstream is generally about 7.4. Hence, particles can experience a broad range of conditions within a biological system, ranging from very acidic (pH 2) to mildly alkaline (pH 8).

The SPR bands of conjugates (Figure 7) were evaluated within the range of pH from 2 to 10, immediately following dilution into each pH buffer solution (f = 10). Since all dendron conjugates precipitated at pH 2 those results are omitted.

As shown in Figure 7, at pH 3 the SPR bands were generally observed to red shift ($\Delta\lambda_{max}$ = 25 to 45 nm), which suggests formation of aggregates. In general, conjugates were unstable under highly acidic conditions ($\leq$4) and stable from mildly acidic to basic conditions (pH $\geq$ 6). In lowering the pH into the acidic range, the negatively charged conjugates are effectively neutralized by protonation of the carboxyl termini ($pK_a \approx 4$). Consequently, a decrease in electrostatic repulsion should lead to decreased stability resulting in aggregation.[93] However, the electrostatic repulsive forces associated with the charged deprotonated carboxyls is also effectively screened at high salt concentrations (e.g., in PBS), yet this has been shown not to cause significant short-term loss of stability. This suggests there are other factors involved, one of which could be an increase in hydrogen bonding between protonated carboxyl termini at pH values near or below their pK_a; carboxyls are known to self-associate when fully protonated.[94] Another possibility is that highly acidic solutions reduce the chemical stability of the Au−S bond that anchors the dendrons to the Au surface; loss of chemical stability would lead subsequently to a loss of colloidal stability as the protective layer is degraded.

Conjugates and citrate-capped AuNPs exhibit distinctly different stability behavior in strongly acidic media (pH 3). The SPR absorption spectrum for citrate-capped AuNPs evolves over time (see Figure 8a), such that the characteristic peak near 520 nm decreases in magnitude and a broader absorption peak gradually develops between (650 and 670) nm. This suggests the coexistence of two physical states, with the primary particle population being depleted at the expense of larger aggregates. On the other hand, for **Au-TA-G1-COOH** at pH 3 (Figure 8b), the SPR peak shows a rapid red shift during the initial 2 h, eventually stabilizing near 560 nm; the SPR peak then decreases in intensity but does not red shift further. This suggests the rapid formation of a new physical state (i.e., clusters) that are then relatively stable toward further physical modification.

DLS measurements conducted under the same conditions at pH 3 (Figure 8c) correlate with the previous SPR results. The

dx.doi.org/10.1021/cm200591h |*Chem. Mater.* 2011, 23, 2665–2676

z-average size of citrate-capped AuNPs continuously increased over time; however, the **Au-TA-G1-COOH** size increased to about 90 nm during the first 2 h, after which it exhibited a relatively slow but steady increase. It should be noted that within ≈24 h citrate-capped AuNPs crashed out of solution, forming a black precipitate that settled to the bottom of the cell. In contrast, the solution of modified conjugates gradually became purple in appearance, then settled out of solution after several days.

AFM height and phase images (obtained after 48 h) for the acidified citrate-capped AuNPs (Figure 8d,e) clearly show large aggregate structures with Au cores apparently fused or in direct contact. In contrast, the acidified **Au-TA-G1-COOH** conjugate (Figure 8f,g) is characterized by small clusters of a few primary particles with distinct cores still visible (i.e., core fusion is not apparent in the AFM image).

The combined UV−vis, DLS and AFM results suggest that citrate primarily provides stability for AuNPs via electrostatic repulsion arising from deprotonated carboxyl groups at pH values above the pK_a, and that because of the small size of citrate, under acidic conditions citrate provides no protection against aggregation thus leading to relatively rapid intercore fusion. Whether the citrate is actually displaced under these conditions, or is simply neutralized by the acid, is not clear and would require additional experiments beyond the scope of the present work. In contrast, the acidified **Au-TA-G1-COOH** conjugate provides both electrostatic repulsion and a stable steric protective layer that prevents intercore fusion under acidic conditions. Thus clusters formed with **Au-TA-G1-COOH**-protected AuNPs initially form weak agglomerates rather than fused aggregates (Figure 8h). Moreover, the conjugates exhibit excellent stability (based on DLS and SPR results) over the pH range from mildly acidic to mildly alkaline (i.e., pH 4 to pH 10); see for instance Figure S4 (see the Supporting Information).

Nanomaterial formulations intended for therapeutic application are most often intravenously infused. An appropriate neutral, hydrophilic, and stable coating minimizes protein binding to the particle, reduces immune system recognition, and prolongs systemic circulation to localize in tumor tissue through enhanced permeability and retention. Because serum contains thiolated proteins that can potentially replace the surface bound gold−thiol bonds and thereby facilitate reticuloendothelial system recognition and uptake, an ideal nanoparticle carrier should have a stable coating resistant to such displacement. Hence, the relative chemical resistances of different surface bound dendritic ligands were investigated. It is well-documented that cyanide ion (CN^-) acts as a strong complexing ligand for Au(I) ions, to the extent that addition of KCN rapidly etches Au surfaces on the basis of Elsner's reaction[95]

$$4Au + 8CN^- + O_2 + 2H_2O \rightarrow 4Au(CN)_2^- + 4OH^-$$

Digestion of Au colloids by cyanide ions is therefore a useful means to evaluate the chemical stability of Au conjugates. When CN^- is able to access the AuNP surface, the characteristic ruby-red color gradually changes to a colorless solution by formation of the soluble $Au(CN)_2^-$ complex. In classical evaluations of cyanide digestion of modified Au colloids by Whitesides,[90] Murray,[96] and Rotello,[97] longer or bulkier alkylmonothiol shells protected the Au core from cyanide attack more efficiently (relative to less bulkier shells) by providing a thicker steric barrier against CN^- approach to the Au surface (see the branch effect, in Figure 9a).

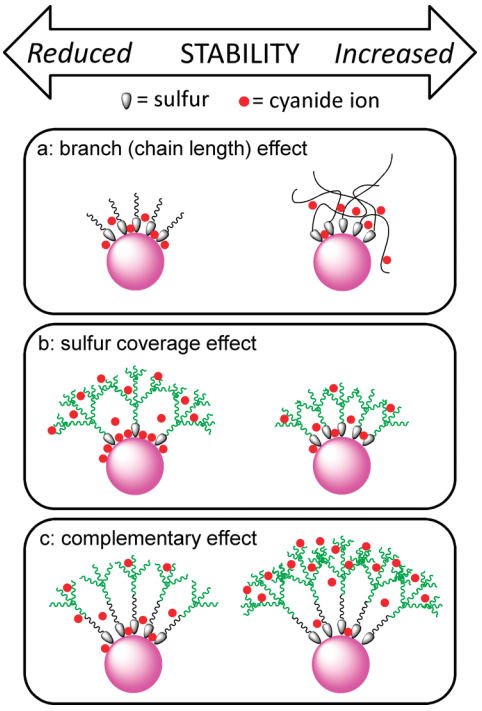

Figure 9. Cartoon depiction of the effects induced by surface conformation of functionalized AuNPs in resisting cyanide ions: (a) branch or chain length effect; (b) sulfur coverage effect; (c) complementary effects.

On the other hand, Fox[69] and Smith[70] have previously reported that smaller dendron−Au conjugates (prepared by reduction of $HAuCl_4$ with disulfide dendrons present) were more stable than larger dendrons, an inverse ligand-molecular mass relationship compared to the classical alkylthiol protected Au. These authors suggested that during the ligation process, small dendrons form "close-packed" conjugates, sterically resisting access of CN^- to the Au core, whereas larger dendrons resulted in "loose-packed" conjugates that allowed greater access to CN^- (see the sulfur coverage effect in Figure 9b), even as the shell "thickness" increased. Recently however, Shon et al.[74] have observed that higher generation (i.e., more bulky) dendron-stabilized AuNPs have superior stability against chemical etching. We hypothesize that this improvement in resistance to KCN etching is correlated to the S/Au ratio of their conjugates−sulfur coverage effect−which should be identical for all AuNP−dendron conjugates in their study (prepared by convergent dendritic functionalization of the **Au-MUA** analog as a starting core material, see Figure 9c).

In the present work, aqueous solutions of the conjugates were rapidly diluted (f = 10) with an aqueous KCN solution (2.0 mmol/L), then decay of the optical density at 520 nm was observed over time (Figure 10). The rate constants for decay (k_1, Table 2) were obtained from a general first-order equation, $y = y' + a\exp(-k_1 t)$, where y is the observed absorbance as a function of time and y' is a correction for light scattering by the finely suspended byproduct (assumed to be constant).[96] The rate constant for citrate-capped AuNPs is not given because of the very rapid loss of optical density.

As shown in Figure 10, citrate-capped AuNPs were dissolved almost immediately upon treatment with KCN solution. The decay rate for **Au-G2-COOH** (Table 2) was observed to be slower than that of **Au-G1-COOH** because of the protection efficiency of the

dx.doi.org/10.1021/cm200591h |*Chem. Mater.* 2011, 23, 2665–2676

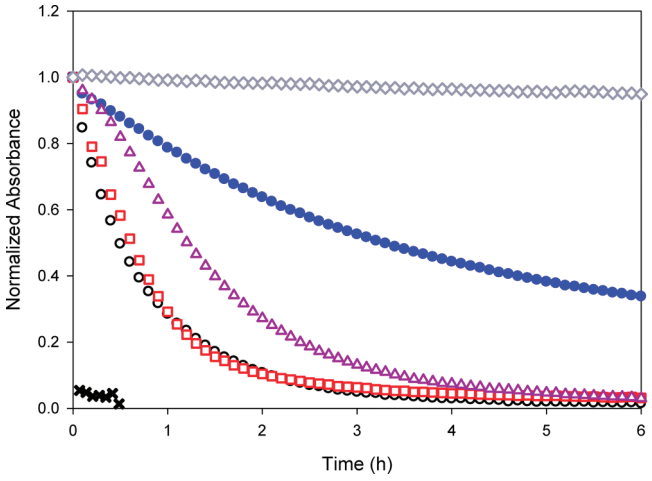

Figure 10. Normalized absorbance decay at 520 nm for AuNPs following treatment with 2.0 mmol/L KCN solution: (×) citrate-capped AuNPs, (○) **Au-G1-COOH**, (□) **Au-G2-COOH**, (△) **Au-SH-G1-COOH**, (●) **Au-TA-G1-COOH**, and (◊) **Au-MUA**.

Table 2. First-Order Decay Rate Constants (k_1) of Optical Density at 520 nm for Conjugates Following Treatment with 2.0 mmol/L KCN Solution

conjugate	k_1 (s^{-1})
Au-G1-COOH	3.7×10^{-4}
Au-G2-COOH	3.2×10^{-4}
Au-SH-G1-COOH	1.2×10^{-4}
Au-TA-G1-COOH	7.1×10^{-5}
Au-MUA	7.7×10^{-6}

bulkier dendrons on the Au surface, suggesting a classical branch effect. However, notwithstanding the presence of a thicker outer shell for **Au-G2-COOH**, the difference between decay rates for **Au-G1-COOH** and **Au-G2-COOH** is very small. The thicker shell is apparently counterbalanced by a S coverage (surface density) for **Au-G2-COOH** that is about half that for **Au-G1-COOH** based on XPS measurements (Table 1). This indicates that not only the branch effect but also the S/Au ratio (S coverage effect) is significant with respect to chemical stability of conjugates in this thiol-anchored dendron system. The S coverage effect is clearly stronger relative to the branch effect, as exemplified by the low rate constants for **Au-SH-G1-COOH** (relative surface coverage ≈0.76) and **Au-TA-G1-COOH** (≈ 0.93) under cyanide digestion. If, for purposes of comparison, S/Au values are assumed to be equivalent to the density of dendron molecules on the Au surface, then **Au-SH-G1-COOH** and **Au-TA-G1-COOH** have effectively 2.3 (0.76 × 3) and 1.4 (0.93/2 × 3) terminal branches, respectively. So, if the branch effect were dominant, **Au-SH-G1-COOH** should be more resistive to KCN etching than **Au-TA-G1-COOH**; however, the results give clear evidence of the predominance of the S coverage effect for thiol bonded dendron conjugates in this system. The decay rate constant for **Au-MUA** (Table 2) as a control (relative surface coverage = 1.0, Table 1) strongly supports this hypothesis.

Finally, long-term stability (i.e., shelf life) is an important parameter for utilization of AuNPs as reference or study materials. Such use requires a stability horizon of 1 to 3 years, at a minimum, in order to be considered viable. The dendron-Au conjugates described herein exhibited excellent stability when stored under ambient laboratory conditions for at least 6 months, over which time significant aggregation as detected by changes in particle size (DLS) or SPR spectra (UV−vis) was largely absent. This result suggests the expectation for reasonable shelf life.

Because dry storage is often more suitable for long-term stability, relative to aqueous-based suspensions, we examined the use of lyophilization to prepare semidry conjugates by removal of the solution phase. To evaluate the efficacy of this approach, we subjected the conjugates to a lyophilization-reconstitution cycle using the citrate-capped AuNPs as a reference point. After lyophilization, citrate-capped AuNPs were highly aggregated when resuspended in DI water (see Figure S5 in the Supporting Information), as indicated by the dark gray color and presence of black precipitate. In contrast, all dendron−Au conjugates yielded dispersible suspensions, albeit with increased mean particle size and a broadened size distribution (see Figure S5 in the Supporting Information).

Post-resuspension analysis by DLS showed a significant increase in the *z*-average size (see Table S1 in the Supporting Information) for all dendron conjugates (ranging from about 100% to 300% of the prelyophilization size), with an obviously broadened intensity-weighted distribution (see for example the hatch marked distribution in Figure S6a in the Supporting Information). Similarly, the SPR peak was slightly red-shifted (see Figure S6b in the Supporting Information, Δ = 2−4 nm) after resuspension, with a small but noticeable increase in absorbance at wavelengths above about 600 nm. Despite the apparent increase in size, these conjugates produce a red translucent suspension indicative of stable AuNPs. These results suggest that some residual agglomerates persist following lyophilization−resuspension, but that most of the material reconstitutes as singlet particles (see the volume weighted distribution, solid line, in Figure S6a in the Supporting Information). The results of this preliminary examination suggest that it may be possible to lyophilize the dendron−Au conjugates for long-term storage. However, the process would require optimization and perhaps the use of excipients to fully prevent irreversible drying-induced agglomeration, and this is beyond the scope of the current study.

CONCLUSIONS

In this study, we report the synthesis of a new series of Newkome-type dendrons designed with consideration of several factors (i.e., generation number, steric effects, number of sulfur atoms per molecule, hydrophilicity, and surface functionality) and intended for ligand exchange reaction with AuNPs. Dendron stabilized AuNPs were successfully prepared by reacting dendron modifiers with commercially available citrate-capped AuNPs, resulting in narrow size distribution conjugates. Physicochemical properties of AuNP-dendron conjugates, such as hydrodynamic size, size distributions and uniformity, stability, and relative S surface coverage (as determined by S/Au ratios), were characterized using a combination of measurement techniques (DLS, AFM, UV−vis, and XPS). Interestingly, XPS analysis revealed that the steric effect induced by molecular structures associated with the dendrons limited the surface coverage of the resulting conjugates. Generally, all AuNP-dendrons exhibited a stable shelf life, temperature independent stability, and, additionally, most dendron encapsulated particles survived against a lyophilization-reconstitution cycle with minimal aggregation compared with native citrate-capped AuNPs (which strongly aggregate and do

not reconstitute). On the other hand, AuNP−dendrons are unstable under strongly acidic conditions, but exhibit excellent stability under slightly acidic to basic conditions. Furthermore, the instability of the conjugates under strongly acidic conditions over time could be differentiated from the behavior exhibited by the native citrate-capped AuNPs, suggesting different destabilization mechanisms are active in each case. Overall, a larger S/Au ratio on the AuNP−dendron surface improves stability for the conjugates under physiological conditions. The stability of conjugates in different media, particularly in PBS was excellent, thereby enhancing their potential for exploitation in biomedical applications ranging from hypothesis testing to functionally dense drug-delivery platforms to downstream conjugation to biological or small molecule drugs and targeting molecules. Finally, evaluation of chemical resistance against cyanide digestion provides evidence to support the presence of both a branch effect and a sulfur coverage effect as described above, but reveals that the sulfur coverage effect is dominant with respect to protecting the AuNP surface from attack by strong ligands such as KCN.

■ ASSOCIATED CONTENT

Ⓢ Supporting Information. Supportive analytical data (^{1}H, ^{13}C NMR, and MALDI-TOF), AFM images, size distributions, UV−vis spectra, and procedures for dendron and corresponding AuNP conjugate preparation. This material is available free of charge via the Internet at http://pubs.acs.org.

■ AUTHOR INFORMATION

Corresponding Author

*Tel: 301-975-5790. Fax: 301-975-5334. E-mail: vince.hackley@nist.gov.

■ ACKNOWLEDGMENT

The authors thank Dr. John T. Simpson and Mr. Sonny Man of the Protein Chemistry Laboratory and the Nanotechnology Characterization Laboratory, respectively, for help in performing MALDI-TOF mass spectrometer measurements used in this study. Their laboratories operate under the Advanced Technology Program, SAIC-Frederick, Inc., for the National Cancer Institute at Frederick. This project has been funded in part by the National Cancer Institute, National Institutes of Health, under Contract HHSN261200800001E. The content of this publication does not necessarily reflect the views or policies of the Department of Health and Human Services.

■ REFERENCES

(1) Niemeyer, C. M. *Angew. Chem., Int. Ed.* **2001**, *40*, 4128–4158.
(2) Hamley, I. W. *Angew. Chem., Int. Ed.* **2003**, *42*, 1692–1712.
(3) Whitesides, G. M. *Small* **2005**, *1*, 172–179.
(4) De, M.; Ghosh, P. S.; Rotello, V. M. *Adv. Mater.* **2008**, *20*, 4225–4241.
(5) Katz, E.; Willner, I. *Angew. Chem., Int. Ed.* **2004**, *43*, 6042–6108.
(6) Shenhar, R.; Rotello, V. M. *Acc. Chem. Res.* **2003**, *36*, 549–561.
(7) Hone, D. C.; Walker, P. I.; Evans-Gowing, R.; FitzGerald, S.; Beeby, A.; Chambrier, I.; Cook, M. J.; Russell, D. A. *Langmuir* **2002**, *18*, 2985–2987.
(8) Choi, M.-R.; Stanton-Maxey, K. J.; Stanley, J. K.; Levin, S. S.; Bardhan, R.; Akin, D.; Badve, S.; Sturgis, J.; Robinson, J. P.; Bashir, R.; Halas, N. J.; Clare, S. E. *Nano Lett.* **2007**, *7*, 3759–3765.
(9) Bergen, J. M.; Von Recum, H. A.; Goodman, T. T.; Massey, A. P.; Pun, S. H. *Macromol. Biosci.* **2006**, *6*, 506–516.
(10) El-Sayed, I. H.; Huang, X. H.; El-Sayed, M. A. *Nano Lett.* **2005**, *5*, 829–834.
(11) Eck, W.; Craig, G.; Sigdel, A.; Ritter, G.; Old, L. J.; Tang, L.; Brennan, M. F.; Allen, P. J.; Mason, M. D. *Acs Nano* **2008**, *2*, 2263–2272.
(12) Rosi, N. L.; Mirkin, C. A. *Chem. Rev.* **2005**, *105*, 1547–1562.
(13) Sonvico, F.; Dubernet, C.; Colombo, P.; Couvreur, P. *Curr. Pharm. Des.* **2005**, *11*, 2091–2105.
(14) Storhoff, J. J.; Mirkin, C. A. *Chem. Rev.* **1999**, *99*, 1849–1862.
(15) Alivisatos, A. P.; Johnsson, K. P.; Peng, X. G.; Wilson, T. E.; Loweth, C. J.; Bruchez, M. P.; Schultz, P. G. *Nature* **1996**, *382*, 609–611.
(16) He, H.; Xie, C.; Ren, J. *Anal. Chem.* **2008**, *80*, 5951–5957.
(17) Mirkin, C. A.; Letsinger, R. L.; Mucic, R. C.; Storhoff, J. J. *Nature* **1996**, *382*, 607–609.
(18) Popovtzer, R.; Agrawal, A.; Kotov, N. A.; Popovtzer, A.; Balter, J.; Carey, T. E.; Kopelman, R. *Nano Lett.* **2008**, *8*, 4593–4596.
(19) Sharma, P.; Brown, S. C.; Bengtsson, N.; Zhang, Q. Z.; Walter, G. A.; Grobmyer, S. R.; Santra, S.; Jiang, H. B.; Scott, E. W.; Moudgil, B. M. *Chem. Mater.* **2008**, *20*, 6087–6094.
(20) Neely, A.; Perry, C.; Varisli, B.; Singh, A. K.; Arbneshi, T.; Senapati, D.; Kalluri, J. R.; Ray, P. C. *Acs Nano* **2009**, *3*, 2834–2840.
(21) Mei, B. C.; Susumu, K.; Medintz, I. L.; Delehanty, J. B.; Mountziaris, T. J.; Mattoussi, H. *J. Mater. Chem.* **2008**, *18*, 4949–4958.
(22) O'Neal, D. P.; Hirsch, L. R.; Halas, N. J.; Payne, J. D.; West, J. L. *Cancer Letters* **2004**, *209*, 171–176.
(23) Prencipe, G.; Tabakman, S. M.; Welsher, K.; Liu, Z.; Goodwin, A. P.; Zhang, L.; Henry, J.; Dai, H. J. *J. Am. Chem. Soc.* **2009**, *131*, 4783–4787.
(24) Daniel, M. C.; Astruc, D. *Chem. Rev.* **2004**, *104*, 293–346.
(25) Frens, G. *Nat. Phys. Sci.* **1973**, *241*, 20–22.
(26) Hao, E.; Schatz, G. C.; Hupp, J. T. *J. Fluoresc.* **2004**, *14*, 331–341.
(27) Turkevitch, J.; Stevenson, P. T.; Hiller, J. *Discuss. Faraday Soc.* **1951**, *11*, 55–75.
(28) Brust, M.; Fink, J.; Bethell, D.; Schiffrin, D. J.; Kiely, C. *J. Chem. Soc., Chem. Commun.* **1995**, 1655–1656.
(29) Murphy, C. J.; San, T. K.; Gole, A. M.; Orendorff, C. J.; Gao, J. X.; Gou, L.; Hunyadi, S. E.; Li, T. *J. Phys. Chem. B* **2005**, *109*, 13857–13870.
(30) Pileni, M. P. *Nat. Mater.* **2003**, *2*, 145–150.
(31) Xia, Y. N.; Yang, P. D.; Sun, Y. G.; Wu, Y. Y.; Mayers, B.; Gates, B.; Yin, Y. D.; Kim, F.; Yan, Y. Q. *Adv. Mater.* **2003**, *15*, 353–389.
(32) Voevodin, A. A.; Vaia, R. A.; Patton, S. T.; Diamanti, S.; Pender, M.; Yoonessi, M.; Brubaker, J.; Hu, J. J.; Sanders, J. H.; Phillips, B. S.; MacCuspie, R. I. *Small* **2007**, *3*, 1957–1963.
(33) Chen, M. S.; Goodman, D. W. *Science* **2004**, *306*, 252–255.
(34) Eustis, S.; El-Sayed, M. A. *Chem. Soc. Rev.* **2006**, *35*, 209–217.
(35) Haes, A. J.; Hall, W. P.; Chang, L.; Klein, W. L.; Van Duyne, R. P. *Nano Lett.* **2004**, *4*, 1029–1034.
(36) Haynes, C. L.; Van Duyne, R. P. *J. Phys. Chem. B* **2001**, *105*, 5599–5611.
(37) Link, S.; El-Sayed, M. A. *J. Phys. Chem. B* **1999**, *103*, 4212–4217.
(38) Nie, S. M.; Emery, S. R. *Science* **1997**, *275*, 1102–1106.
(39) Su, K. H.; Wei, Q. H.; Zhang, X.; Mock, J. J.; Smith, D. R.; Schultz, S. *Nano Lett.* **2003**, *3*, 1087–1090.
(40) Thomas, J. M.; Johnson, B. F. G.; Raja, R.; Sankar, G.; Midgley, P. A. *Acc. Chem. Res.* **2003**, *36*, 20–30.
(41) Newkome, G. R.; Moorefield, C. N.; Vötle, F. *Dendrimers and Dendrons: Concepts, Syntheses, Applications*; VCH: Weinheim, Germany, 2001.
(42) Frechet, J. M. J.; Tomalia, D. A. *Dendrimers and Other Dendritic Polymers*; John Wiley and Sons: New York, 2002.
(43) Balogh, L.; Tomalia, D. A. *J. Am. Chem. Soc.* **1998**, *120*, 7355–7356.
(44) Zhao, M. Q.; Sun, L.; Crooks, R. M. *J. Am. Chem. Soc.* **1998**, *120*, 4877–4878.

(45) Crooks, R. M.; Zhao, M. Q.; Sun, L.; Chechik, V.; Yeung, L. K. *Acc. Chem. Res.* **2001**, *34*, 181–190.
(46) Smith, D. K. *Chem. Commun.* **2006**, 34–44.
(47) Srivastava, S.; Frankamp, B. L.; Rotello, V. M. *Chem. Mater.* **2005**, *17*, 487–490.
(48) Kim, Y. G.; Oh, S. K.; Crooks, R. M. *Chem. Mater.* **2004**, *16*, 167–172.
(49) Triulzi, R. C.; Micic, M.; Giordani, S.; Serry, M.; Chiou, W. A.; Leblanc, R. M. *Chem. Commun.* **2006**, 5068–5070.
(50) Pan, B.; Gao, F.; Ao, L.; Tian, H.; He, R.; Cui, D. *Colloids Surf., A* **2005**, *259*, 89–94.
(51) Esumi, K.; Ichikawa, M.; Yoshimura, T. *Colloids Surf., A* **2004**, *232*, 249–252.
(52) Balogh, L.; Valluzzi, R.; Laverdure, K. S.; Gido, S. P.; Hagnauer, G. L.; Tomalia, D. A. *J. Nanopart. Res.* **1999**, *1*, 353–368.
(53) Satoh, K.; Yoshimura, T.; Esumi, K. *J. Colloid Interface Sci.* **2002**, *255*, 312–322.
(54) Knecht, M. R.; Garcia-Martinez, J. C.; Crooks, R. M. *Langmuir* **2005**, *21*, 11981–11986.
(55) Esumi, K.; Akiyama, S.; Yoshimura, T. *Langmuir* **2003**, *19*, 7679–7681.
(56) Chechik, V.; Crooks, R. M. *Langmuir* **1999**, *15*, 6364–6369.
(57) Bielinska, A.; Eichman, J. D.; Lee, I.; Baker, J. R., Jr.; Balogh, L. *J. Nanopart. Res.* **2002**, *4*, 395–403.
(58) Grohn, F.; Bauer, B. J.; Akpalu, Y. A.; Jackson, C. L.; Amis, E. J. *Macromolecules* **2000**, *33*, 6042–6050.
(59) Esumi, K.; Hosoya, T.; Suzuki, A.; Torigoe, K. *Langmuir* **2000**, *16*, 2978–2980.
(60) Park, M. H.; Ofir, Y.; Samanta, B.; Rotello, V. M. *Adv. Mater.* **2009**, *21*, 2323–2327.
(61) Pietsch, T.; Appelhans, D.; Gindy, N.; Voit, B.; Fahmi, A. *Colloids Surf., A* **2009**, *341*, 93–102.
(62) Advincula, R. C. *Dalton Trans.* **2006**, 2778–2784.
(63) Daniel, M. C.; Ruiz, J.; Nlate, S.; Blais, J. C.; Astruc, D. *J. Am. Chem. Soc.* **2003**, *125*, 2617–2628.
(64) Wang, R. Y.; Yang, J.; Zheng, Z. P.; Carducci, M. D.; Jiao, J.; Seraphin, S. *Angew. Chem., Int. Ed.* **2001**, *40*, 549–552.
(65) Nakao, S.; Torigoe, K.; Kon-No, K.; Yonezawa, T. *J. Phys. Chem. B* **2002**, *106*, 12097–12100.
(66) Kim, M. K.; Jeon, Y. M.; Jeon, W. S.; Kim, H. J.; Hong, S. G.; Park, C. G.; Kim, K. *Chem. Commun.* **2001**, 667–668.
(67) Li, D.; Li, J. *Colloids Surf., A* **2005**, *257−258*, 255–259.
(68) Gopidas, K. R.; Whitesell, J. K.; Fox, M. A. *J. Am. Chem. Soc.* **2003**, *125*, 14168–14180.
(69) Gopidas, K. R.; Whitesell, J. K.; Fox, M. A. *J. Am. Chem. Soc.* **2003**, *125*, 6491–6502.
(70) Love, C. S.; Ashworth, I.; Brennan, C.; Chechik, V.; Smith, D. K. *J. Colloid Interface Sci.* **2006**, *302*, 178–186.
(71) Komine, Y.; Ueda, I.; Goto, T.; Fujihara, H. *Chem. Commun.* **2005**, 302–304.
(72) Daniel, M. C.; Aranzaes, J. R.; Nlate, S.; Astruc, D. *J. Inorg. Organomet. Polym. Mater.* **2005**, *15*, 107–119.
(73) Koenig, S.; Chechik, V. *Langmuir* **2003**, *19*, 9511–9517.
(74) Shon, Y. S.; Choi, D.; Dare, J.; Dinh, T. *Langmuir* **2008**, *24*, 6924–6931.
(75) Huang, B. H.; Tomalia, D. A. *J. Lumin.* **2005**, *111*, 215–223.
(76) DeMattei, C. R.; Huang, B. H.; Tomalia, D. A. *Nano Lett.* **2004**, *4*, 771–777.
(77) Shi, X. Y.; Sun, K.; Baker, J. R. *J. Phys. Chem. C* **2008**, *112*, 8251–8258.
(78) Nuraje, N.; Su, K.; Samson, J.; Haboosheh, A.; MacCuspie, R. I.; Matsui, H. *Supramol. Chem.* **2006**, *18*, 429–434.
(79) Hackley, V. A.; Clogston, J. D. *Measuring the Size of Nanoparticles in Aqueous Media Using Batch-Mode Dynamic Light Scattering*; NIST-NCL Joint Assay Protocol PCC-1 2008; National Cancer Institute, Nanotechnology Characterization Laboratory: Frederick, MD, 2008.
(80) Newkome, G. R.; Weis, C. D.; Moorefield, C. N.; Fronczek, F. R. *Tetrahedron Lett.* **1997**, *38*, 7053–7056.
(81) Newkome, G. R.; Behera, R. K.; Moorefield, C. N.; Baker, G. R. *J. Org. Chem.* **1991**, *56*, 7162–7167.
(82) Kelly, K. L.; Coronado, E.; Zhao, L. L.; Schatz, G. C. *J. Phys. Chem. B* **2003**, *107*, 668–677.
(83) Min, G. K.; Bevan, M. A.; Prieve, D. C.; Patterson, G. D. *Colloids Surf., A* **2002**, *202*, 9–21.
(84) Koppel, D. E. *J. Chem. Phys.* **1972**, *57*, 4814–4820.
(85) Tsai, D. H.; DelRio, F. W.; MacCuspie, R. I.; Cho, T. J.; Zachariah, M. R.; Hackley, V. A. *Langmuir* **2010**, *26*, 10325–10333.
(86) Wang, H.; Chen, S. F.; Li, L. Y.; Jiang, S. Y. *Langmuir* **2005**, *21*, 2633–2636.
(87) Castner, D. G.; Hinds, K.; Grainger, D. W. *Langmuir* **1996**, *12*, 5083–5086.
(88) Tsai, D. H.; Zangmeister, R. A.; Pease, L. F.; Tarlov, M. J.; Zachariah, M. R. *Langmuir* **2008**, *24*, 8483–8490.
(89) Moulder, J. F.; Stickle, W. F.; Sobol, P. E.; Bomben, K. D. *Handbook of X-ray Photoelectron Spectroscopy*; Perkin-Elmer: Eden Prairie, MN, 1995.
(90) Weisbecker, C. S.; Merritt, M. V.; Whitesides, G. M. *Langmuir* **1996**, *12*, 3763–3772.
(91) Mei, B. C.; Oh, E.; Susumu, K.; Farrell, D.; Mountziaris, T. J.; Mattoussi, H. *Langmuir* **2009**, *25*, 10604–10611.
(92) Garrett, R. H.; Grisham, C. M. *Biochemistry*; Saunders College Publishing: Fort Worth, 1999.
(93) Zhu, T.; Vasilev, K.; Kreiter, M.; Mittler, S.; Knoll, W. *Langmuir* **2003**, *19*, 9518–9525.
(94) Riemenschneider, W. *Ullmann's Encyclopedia of Industrial Chemistry*; John Wiley and Sons: New York, 2010.
(95) Elsner, L. *J. Prakt. Chem.* **1846**, *37*, 441–446.
(96) Templeton, A. C.; Hostetler, M. J.; Kraft, C. T.; Murray, R. W. *J. Am. Chem. Soc.* **1998**, *120*, 1906–1911.
(97) Paulini, R.; Frankamp, B. L.; Rotello, V. M. *Langmuir* **2002**, *18*, 2368–2373.